IEEE Access
Multidisciplinary | Rapid Review | Open Access Journal

Received October 24, 2018, accepted November 2, 2018, date of publication November 9, 2018,
date of current version December 7, 2018.

Digital Object Identifier 10.1109/ACCESS.2018.2880209

Study on a Cylindrical Sensor Network for Intelligent Health Monitoring and Prognosis

YANG LI AND MIN ZHANG

Tianjin Key Laboratory of Wireless Mobile Communications and Power Transmission, Tianjin Normal University, Tianjin 300387, China

Corresponding author: Yang Li (liyang_tongxin@163.com)

This work was supported by the Tianjin Higher Education Creative Team Funds Program.

ABSTRACT In this paper, intelligent body healthcare management based on body-centric wireless communications (BCWCs) is considered, and a wearable sensor network is studied. The interaction between electromagnetic waves and the human body is studied at 5 GHz. With the development of BCWCs, numerous on-body sensors need to be interconnected and transmitting information about human body healthcare. Structures of uniform cylindrical sensor networks for intelligent health monitoring and prognosis are proposed and studied. The reason for choosing a cylindrical sensor network is that the shape of a human torso can be approximated as a cylinder. Different numbers and arrangements of wearable antennas are considered and compared, and the far-field beam pattern is considered an important indicator in the investigation. Finally, a sparse cylindrical antenna array is also proposed, and good directional beam pattern performance is obtained. Electromagnetic simulation is performed mainly by the finite-difference time-domain method. This paper provides guidelines for the arrangement of wearable sensor networks.

INDEX TERMS Intelligent body healthcare management, on-body wireless communication, wearable sensor network, uniform cylindrical antenna array, antenna arrangement.

I. INTRODUCTION

Recently, communication technology has become increasingly important in the application of intelligent body healthcare management. Intelligent body healthcare management is based on body-centric wireless communications (BCWCs), which mainly include two kinds of systems, wearable electronic systems and implantable electronic systems [1]. Through wearable electronic systems and implantable electronic systems, we can detect human health indicators such as heart rate, body temperature and blood pressure. There are many studies on body-centric wireless communications [1], [2] in part because we have some previous studies on implantable electronic systems [3]–[5]. In this study, we pay attention to wearable electronic systems. Wearable electronic systems have many application scenarios, such as (1) monitoring of vital signs of bedridden patients in hospitals and (2) monitoring of fitness indicators of athletes in the gym.

In our opinion, if wearable devices operate in the frequency bands of 5G mobile communications, such as 3.3-3.6 GHz and 4.8-5 GHz, it will bring great convenience; for example, one can use mobile phones or a personal digital assistant (PDA) to receive signals emitted by wearable devices. It is important to study the interaction between the human body and electromagnetic waves in the 5G mobile communication band.

There have been many previous studies on sensor networks, and the main purpose of a sensor network is to monitor an area, as is done in target detection, source localization and direction-of arrival estimation. Several researchers have studied sensor networks [6]–[14]. P. P. Vaidyanathan and P. Pal proposed the nested array and the coprime array, which achieved large degrees of freedom and could be represented in closed-form expressions [15], [16]. For the reason that cylindrical sensor arrays usually make use of only a part of the elements at a time, Q. Liang and N. Wu proposed a sparse sensor network constructed of a one-dimensional, two-dimensional and three-dimensional nested cylindrical sensor network, which combined the nested linear array with a uniform circular array [17]–[20]. For the reason that a cylindrical structure is easy to use in human body applications, in this paper, cylindrical antenna arrays are considered for human health monitoring and prognosis. A cylindrical array contains simple z-polarized dipole antennas in three directions, which provide wide cover in both the azimuth plane and the elevation plane. Although microstrip antenna is also suitable for this application, dipole antenna is used to compose

the antenna array in this study for simple. We consider the application of intelligent body healthcare management to study appropriate wearable sensor networks.

In this study, the interaction between electromagnetic waves and the human body at 5 GHz is discussed, a uniform cylindrical antenna array is discussed, and moreover a sparse nested array for intelligent body healthcare management is proposed. The simulation results are carried out by using a 3-D full-wave electromagnetic and computational life sciences simulation software SEMCAD, which is based on the finite-difference time-domain (FDTD) method. The far-field beam pattern is considered an important indicator of the investigation.

This manuscript is organized as follows. A cylindrical human torso phantom with one antenna is shown in Section 2. A two-dimensional one-turn antenna array is introduced in Section 3. In Section 4, the results and analysis of a three-dimensional cylindrical antenna array are described and studied. Finally, the results and observations are summarized in Section 5.

II. CYLINDRICAL HUMAN BODY PHANTOM WITH ONE ANTENNA

Because the shape of a human torso can be approximated as a cylinder, in this study, a simple cylinder is used as the human torso phantom. However, different people have different shapes; therefore, to obtain a generalized conclusion, two phantoms, a LARGE phantom and a THIN phantom, are developed to simulate large people and thin people, respectively.

For the sake of simplicity, muscle can be treated as a homogeneous material of the human body [21], [22], and the relative permittivity and the conductivity of muscle are $\varepsilon_r = 49.5$ and $\sigma = 4$ [S/m] at 5 GHz, respectively [21]. For the LARGE phantom, the perimeter of the circle is 1004.8 mm, and for the THIN phantom, the perimeter of the circle is 753.6 mm, both of which are larger than 10 λ at 5 GHz.

SEMCAD software that was developed and provided by SPEAG is used in this study, and the software is based on the finite-difference time-domain (FDTD) method. A hardware accelerated GPU is used to improve the computing speed and reduce the calculation time. In the FDTD analysis, the number of cells is $302 \times 302 \times 451$, and a Gaussian differential pulse is used as an excitation, and the center frequency is set as 5 GHz. The cell sizes are $\Delta x = \Delta y = \Delta z = 2$ mm. In addition, 11-layer PML is used as an absorbing boundary condition.

Fig. 1 shows the numerical model. A simple half-wavelength z-polarized dipole antenna with length l_1 is placed near the cylindrical human body phantom. Fig. 2 shows the far-field directional beam pattern at 5 GHz; because the conductivity of the human body at 5 GHz is very high, it reflects electromagnetic waves, and the electromagnetic wave is very weak on the opposite side of the antenna ($120° < \varphi < 240°, \theta < 0°$). For example scenario 1, which is mentioned in Section 1, when a patient is wearing a sensor

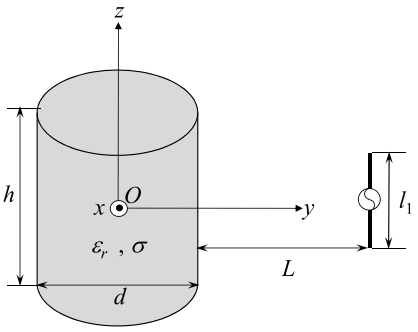

$\varepsilon_r = 49$, $\sigma = 4$ [S/m]; $l_1 = 26$ mm; $L = 20$ mm;
LARGE : $d = 320$ mm, $h = 480$ mm;
THIN : $d = 240$ mm, $h = 480$ mm.

FIGURE 1. A cylindrical human body phantom with a dipole antenna.

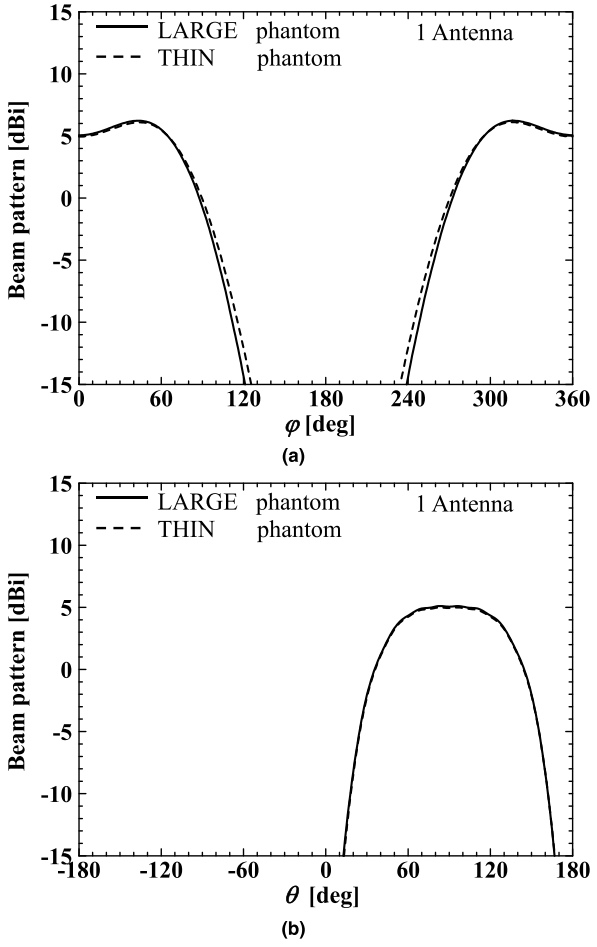

FIGURE 2. Beam pattern of one dipole antenna for the LARGE phantom and the THIN phantom at 5 GHz. (a) Elevation plane. (b) Azimuth plane.

with his or her back to the receiver, or for scenario 2, when an athlete is wearing a sensor with his or her back to the receiver, it is difficult to receive effective signals. Therefore, it is necessary to consider a wearable sensor network consisting of several wearable sensors; in other words, it is important to consider the wearable antenna arrangement.

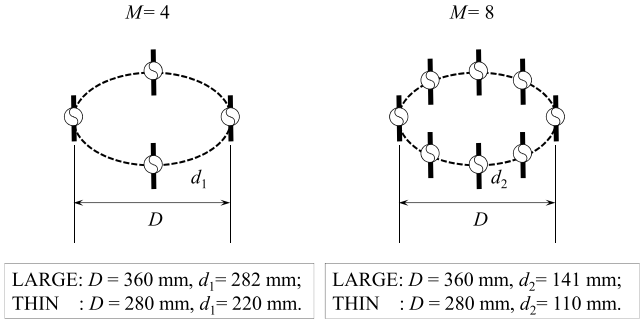

FIGURE 3. One-turn circular antenna array ($N = 1$, $M = 4$ and $M = 8$).

III. ONE-TURN CIRCULAR ANTENNA ARRAY

Fig. 3 shows the one-turn circular antenna array. M represents the number of elements in the circular array. The diameter D = 360 mm and 280 mm, for the LARGE phantom and the THIN phantom, respectively. The distances between two adjacent dipole antenna d_1 and d_2 are:

$$d_1 = \frac{1}{4}\pi D \tag{1}$$

$$d_2 = \frac{1}{8}\pi D \tag{2}$$

The far-field directional beam pattern of the one-turn antenna array ($N = 1$) for the LARGE phantom is shown in Fig. 4. Because of the symmetry of a cylindrical array, only 0°- 180° of the far-field beam pattern is considered. In the azimuth plane (H-plane), the lobes are almost the same, while the maximum magnitude in the case of $M = 8$ is 2-3 dB larger than those in the case of $M = 4$. A large magnitude of the beam pattern indicates large received power. In the azimuth plane (E-plane) the far-field beam patterns are different; in the case of $M = 8$ both the magnitude of the major lobe and the half-power beam width (HPBW) of the major lobe are larger than those in the case of $M = 4$, while in the case of $M = 4$, two large side lobes appear.

The far-field directional beam pattern of the one-turn antenna array ($N = 1$) for the THIN phantom is shown in Fig. 5. In the azimuth plane (H-plane), the lobes are almost the same, while the maximum magnitude in the case of $M = 8$ is 2-3 dB larger than those in the case of $M = 4$. Large magnitude of the beam pattern means large received power. In the azimuth plane (E-plane), the far-field beam patterns are different; in the case of $M = 4$, large magnitude of major lobes appear in the range of $-120° < \theta < -60°$ and $60° < \theta < 120°$, while in the case of $M = 8$, the performance of the directional beam pattern is poor.

IV. CYLINDRICAL ANTENNA ARRAY

Fig. 6 shows a human torso-shaped model with a cylindrical array. The two-dimensional parameters are the same as those in Fig. 3. The number of circular arrays is represented by N, and M is the number of elements in each circular array. In particular, a represents the distance between two adjacent circular arrays.

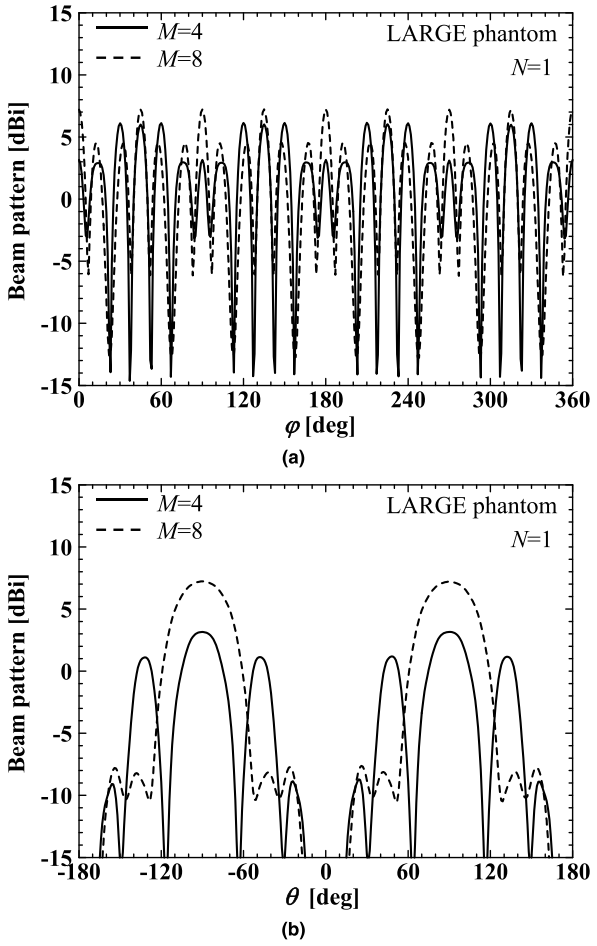

FIGURE 4. Beam pattern with different M for the LARGE model at 5 GHz. (a) Elevation plane. (b) Azimuth plane.

A. DISCUSSION OF A

Fig. 7 shows the directional beam pattern with $a = 1/2\lambda$, λ and 2λ under the condition of $M = 8$ and $N = 3$ for the LARGE phantom. In the elevation plane, both the numbers of lobes and the half-power beam width are almost the same among these conditions, while the maximum magnitudes of beam patterns in the cases of $a = \lambda$ and $a = 2\lambda$ are almost the same, 2 dB larger than that in the case of $a = 1/2\lambda$ ($a = \lambda$ and $a = 2\lambda$: maximum value 12.5 dBi, $\varphi = 45°/90°/135°$; $a = 1/2\lambda$: maximum value 10.5 dBi, $\varphi = 45°/90°/135°$). This phenomenon indicates that under the condition that a is equal to an integer multiple of λ, the same beam pattern will be obtained in the elevation plane. In the azimuth plane, the maximum magnitude of the beam patterns in the case of $a = \lambda$ and $a = 2\lambda$ are almost same (maximum value 12.5 dBi, $\theta = 90°$), while with the increase of a, the half-power beam width becomes narrow ($a = 0.5\lambda$: 76°-104°, HPBW = 28°; $a = \lambda$: 82°-98°, HPBW = 16°; $a = 2\lambda$: 86°-94°, HPBW = 8°), and two large side lobes (maximum value 6.2 dBi, $\theta = 63°/117°$) are obtained in the case of $a = 2\lambda$. The performance of the major lobe shows a tradeoff relationship between the maximum magnitude of the beam pattern and the half-power beam width. If we consider

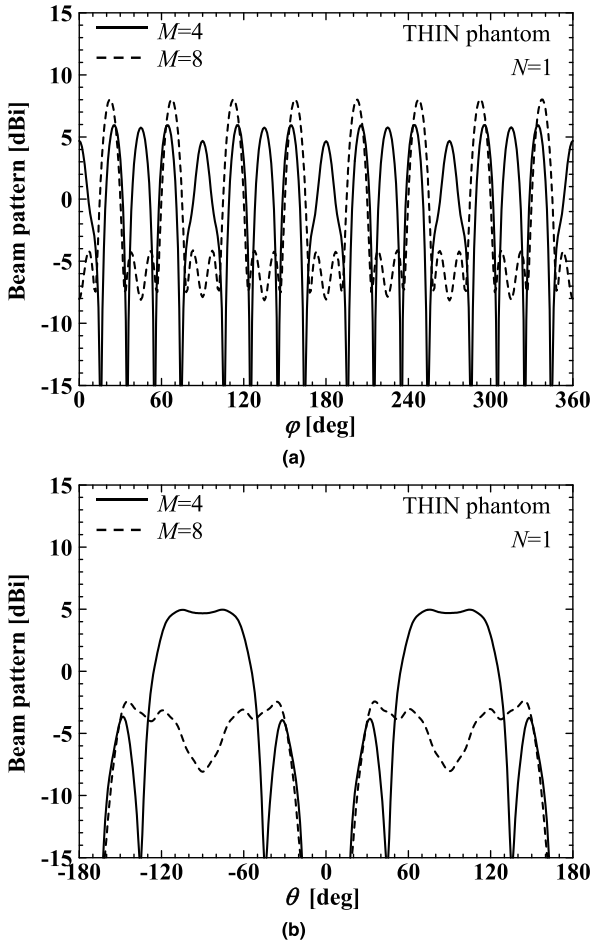

FIGURE 5. Beam pattern with different M for the THIN phantom at 5 GHz. (a) Elevation plane. (b) Azimuth plane.

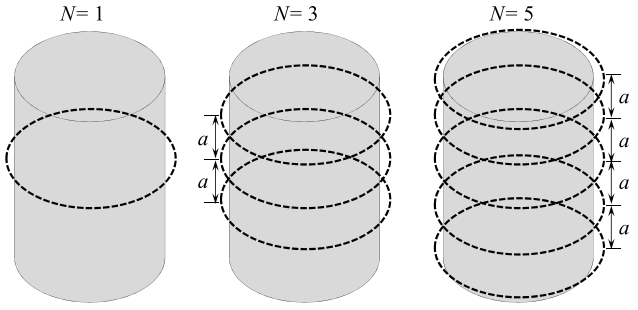

FIGURE 6. A cylindrical human body phantom with a uniform cylindrical antenna array.

both the number of antennas and the quantity of the beam pattern simultaneously, for the LARGE phantom, $a = \lambda$ is a compromise.

Fig. 8 shows the directional beam patterns with $a = 1/2\lambda$, λ and 2λ under the condition of $M = 8$ and $N = 3$ for the THIN phantom. In the elevation plane, the number of lobes are almost the same among these conditions, while the maximum magnitude of the beam pattern is large in the case of $a = \lambda$ ($a = 1/2\lambda$: maximum value 11.6 dBi, $\varphi = 22°/68°$; $a = \lambda$: maximum value 13.5 dBi, $\varphi = 22°/68°$; $a = 2\lambda$: maximum value 12.8 dBi, $\varphi = 22°/68°$). In the

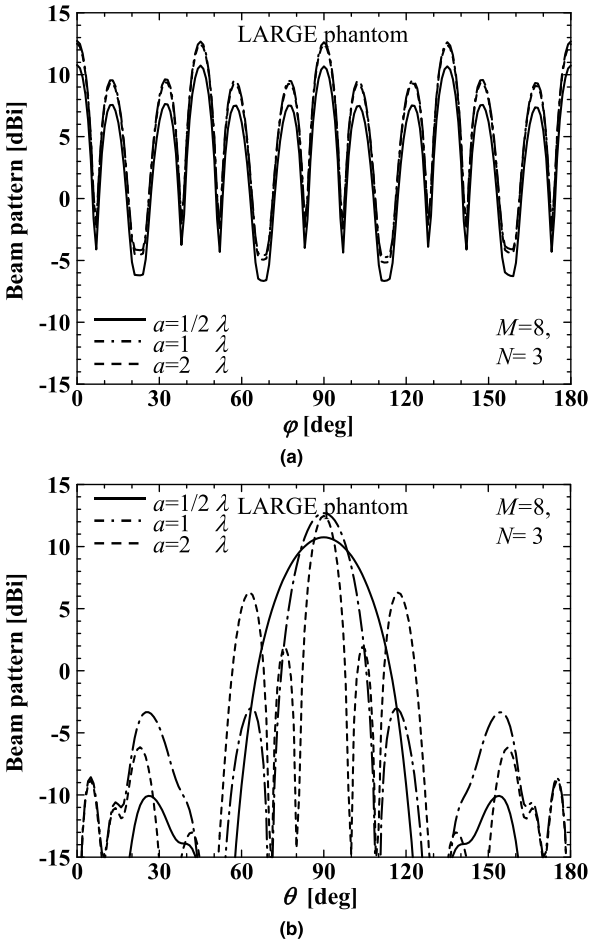

FIGURE 7. Beam pattern with different a values under the condition of $M = 8$ and $N = 3$ for the LARGE phantom at 5 GHz. (a) Elevation plane. (b) Azimuth plane.

azimuth plane, the performance of the major lobe shows a tradeoff relationship between the maximum magnitude of the beam pattern and the half-power beam width ($a = 0.5\lambda$: maximum value -2.8 dBi, $\theta = 34°/146°$; $a = \lambda$: maximum value -0.2 dBi, $\theta = 32°/148°$; $a = 2\lambda$: maximum value 1.9 dBi, $\theta = 60°/130°$). Generally, if we consider both the number of antennas and the quantity of the beam pattern simultaneously, for both the LARGE phantom and the THIN phantom, $a = \lambda$ is a compromise.

B. DISCUSSION OF M AND N

Fig. 9 shows the directional beam patterns with $N = 1$, 3, and 5 under the condition of $M = 4$ and $a = \lambda$ for the LARGE phantom. In the elevation plane, both the number of lobes and the half-power beam width are almost the same among these conditions, while the maximum magnitude of the beam pattern increases as N increases ($N = 1$: maximum value 6.1 dBi, $\varphi = 30°/40°/60°$; $N = 3$: maximum value 11.3 dBi, $\varphi = 30°/40°/60°$; $N = 5$: maximum value 13.7 dBi, $\varphi = 30°/40°/60°$). The performance of the beam pattern in the elevation plane is better under the condition of more antennas. In the azimuth plane, with the

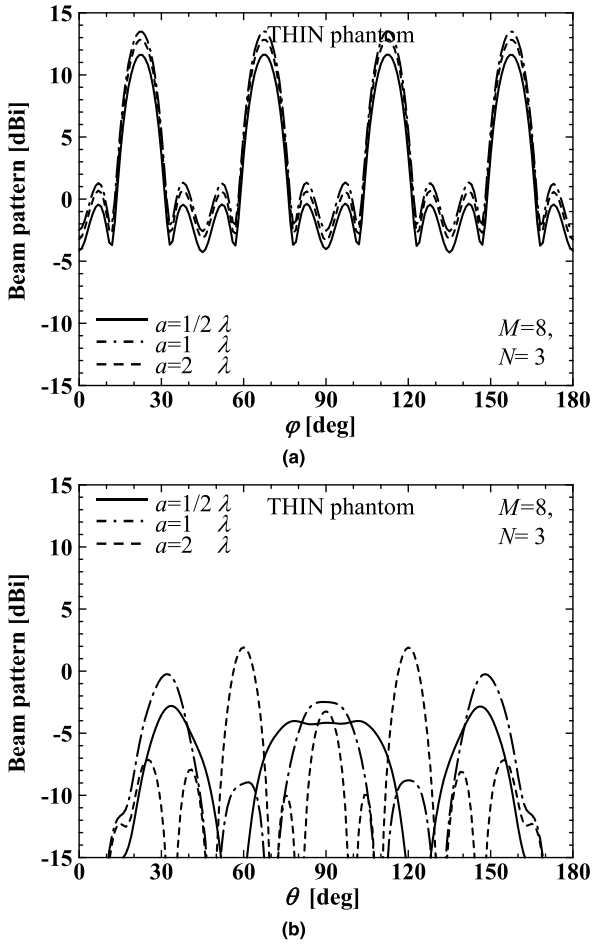

FIGURE 8. Beam pattern with different a values under the condition of $M = 8$ and $N = 3$ for the THIN phantom at 5 GHz. (a) Elevation plane. (b) Azimuth plane.

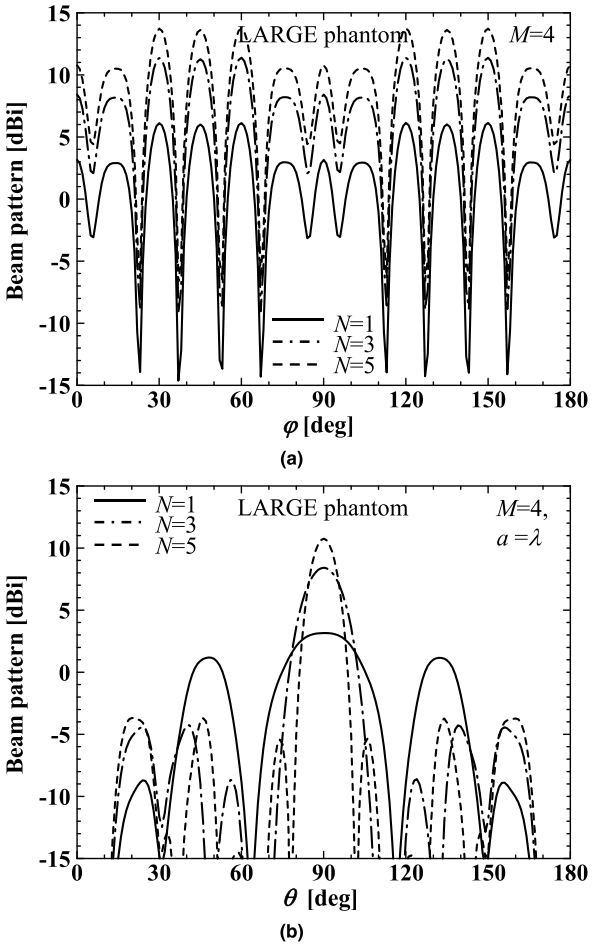

FIGURE 9. Beam pattern with changing N under the condition of $M = 4$ and $a = \lambda$ for the LARGE phantom at 5 GHz. (a) Elevation plane. (b) Azimuth plane.

increase of N, the maximum magnitude of the beam pattern (the major lobe) becomes large ($N = 1$: maximum value 3.2 dBi, $\theta = 90°$; $N = 3$: maximum value 8.4 dBi, $\theta = 90°$; $N = 5$: maximum value 10.7 dBi, $\theta = 90°$), and the half-power beam width becomes narrow ($N = 1$: 75°-105°, HPBW = 30°; $N = 3$: 82°-98°, HPBW = 16°; $N = 5$: 85°-95°, HPBW = 10°). The performance of the major lobe shows a tradeoff relationship between the maximum magnitude of the beam pattern and the half-power beam width.

Fig. 10 shows the directional beam patterns with $N = 1$, 3, and 5 under the condition of $M = 8$ and $a = \lambda$ for the THIN phantom. In the elevation plane, both the number of lobes and the half-power beam width are almost the same among these conditions, while the maximum magnitude of the beam pattern increases as N increases ($N = 1$: maximum value 6.0 dBi, $\varphi = 25°/45°/65°$; $N = 3$: maximum value 11.2 dBi, $\varphi = 25°/45°/65°$; $N = 5$: maximum value 13.6 dBi, $\varphi = 25°/45°/65°$). The performance of the beam pattern in the elevation plane is better under the condition of more antennas. In the azimuth plane, with the increase of N, the maximum magnitude of the beam pattern (the major lobe) becomes large ($N = 1$: maximum value 5.0 dBi, $\theta = 70°/105°$; $N = 3$: maximum value 9.9 dBi, $\theta = 90°$; $N = 5$: maximum value 12.3 dBi, $\theta = 90°$), and the half-power beam width becomes narrow ($N = 1$: 58°-122°, HPBW = 64°; $N = 3$: 81°-99°, HPBW = 18°; $N = 5$: 85°-95°, HPBW = 10°). Comparing between $N = 3$ and $N = 5$, a tradeoff relationship between the maximum magnitude of the beam pattern and the half-power beam width is appeared. A wide half-power beam width (HPBW = 64°) is observed in the case of $N = 1$ while the maximum magnitude of the beam pattern is small (maximum value 5.0 dBi).

Fig. 11 shows the directional beam pattern of $N = 1$, 3, and 5 under the condition of $M = 8$ and $a = \lambda$ for the LARGE phantom. In the elevation plane, both the numbers of lobes and the half-power beam width are almost same among these conditions, while the maximum magnitude of the beam pattern is increased as N increased ($N = 1$: maximum value 7.2 dBi; $N = 3$: maximum value 12.4 dBi; $N = 5$: maximum value 14.7 dBi). The performance of beam pattern in the elevation plane is better under the condition of more antennas. In the azimuth plane, with the increase of N the maximum beam pattern of the major lobe becomes

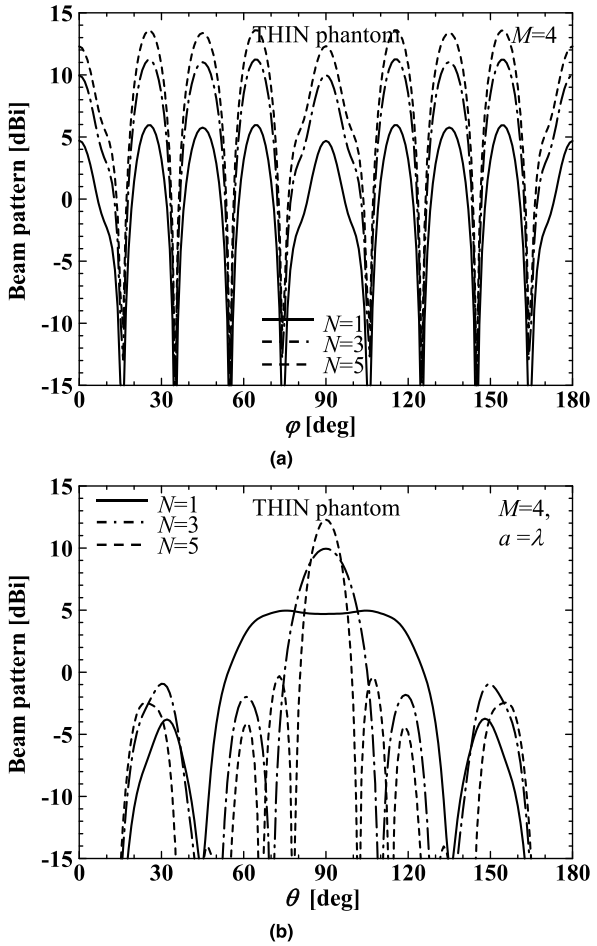

FIGURE 10. Beam pattern with changing N under the condition of $M = 4$ and $a = \lambda$ for the THIN phantom at 5 GHz. (a) Elevation plane. (b) Azimuth plane.

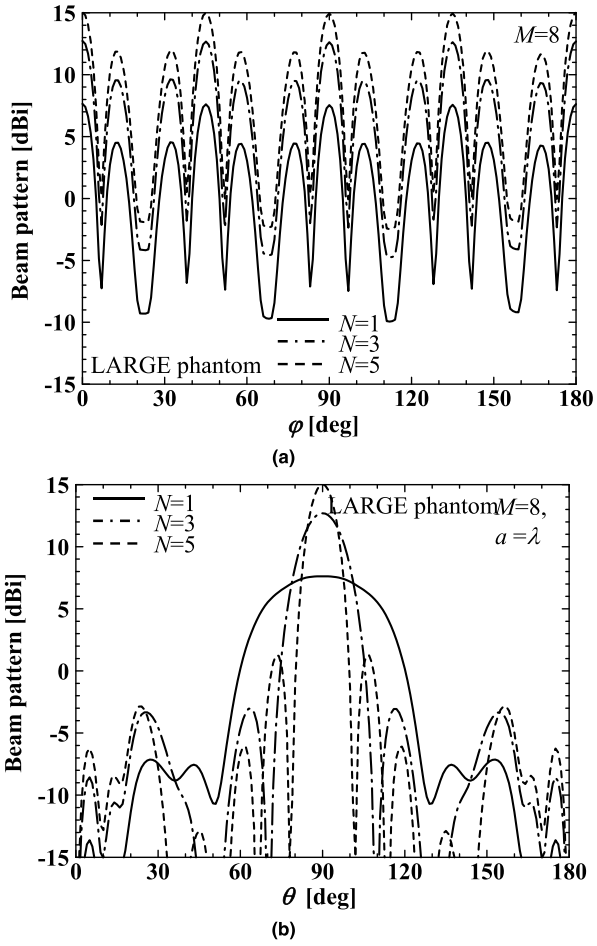

FIGURE 11. Beam pattern with changing N under the condition of $M = 4$ and $a = \lambda$ for the LARGE phantom at 5 GHz. (a) Elevation plane. (b) Azimuth plane.

large ($N = 1$: maximum value 7.2 dBi; $N = 3$: maximum value 12.4 dBi; $N = 5$: maximum value 14.7 dBi; $\theta = 90°$), and the half-power beam width becomes narrow ($N = 1$: 68°-112°, HPBW = 44°; $N = 3$: 82°-98°, HPBW = 16°; $N = 5$: 85°-95°, HPBW = 10°). The performance of the major lobe shows a tradeoff relationship between the maximum magnitude of the beam pattern and the half-power beam width. In the case of $N = 1$, a relatively wide half-power beam width is obtained while in the case of $N = 5$, a relatively large maximum magnitude of the beam pattern is obtained.

In Section 4 A, Fig. 8 shows that under the condition of $M = 8$, for the THIN phantom the performance of the beam pattern is poor, it is recommend that $M = 4$ is an optimum decision.

A simple summary of the discussion regarding changing values of N as follows: in the elevation plane, increasing N can increase the maximum magnitude of the beam pattern; in the azimuth plane, there is a tradeoff relationship between the maximum magnitude of the beam pattern and the half-power beam width. For example, in scenario 1, which is mentioned in Section 1, when a patient is wearing a wearable sensor on a bed (static), a large value of the maximum magnitude is preferred. In contrast, in scenario 2, when an athlete is wearing a wearable sensor during movement (dynamic), a wide half-power beam width is preferred. A simple summary of the discussion regarding changing values of M as follows: for the LARGE phantom in the elevation plane, increasing M can increase the maximum magnitude of the beam pattern; in the azimuth plane, there is a tradeoff relationship between the maximum magnitude of the beam pattern and the half-power beam width; and for the THIN phantom, the performance of the beam pattern in the case of $M = 4$ is better than that in the case of $M = 8$.

C. SPARSE CYLINDRICAL ANTENNA ARRAY

From the results of the uniform cylindrical antenna array, it is found that under the condition that the number of antennas is too small, the signal intensity is not sufficient. However, under the condition that the number of antennas is too large, the antennas will cause mutual interference. To solve this contradiction, an interesting sparse cylindrical antenna array is proposed, under the condition that $M = 4$ and $N = 5$, and the arrangement of antennas is shown in Fig. 12. In the cases

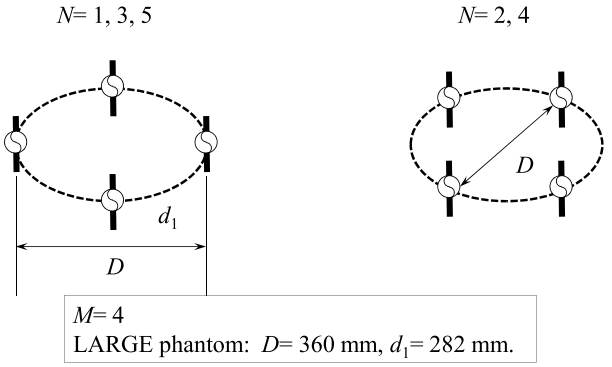

FIGURE 12. Antenna arrangement of the sparse cylindrical antenna array for the LARGE phantom.

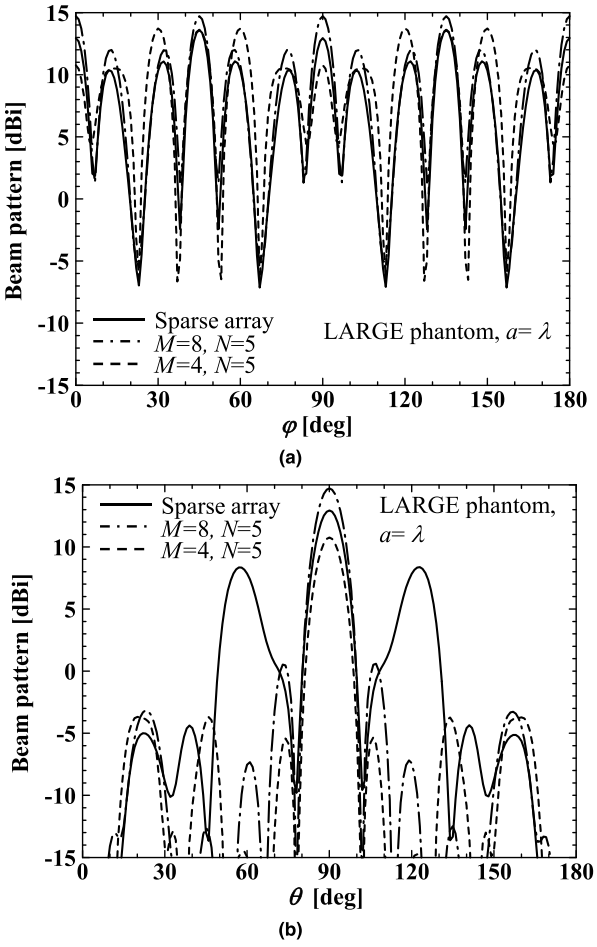

FIGURE 13. Beam pattern of sparse cylindrical antenna array under the condition of $M = 4$, $N = 5$ and $a = \lambda$ for the LARGE phantom at 5 GHz. (a) Elevation plane. (b) Azimuth plane.

of $N = 1$, 3, and 5 the four antennas are located as shown in the left figure, while in the cases of $N = 2$, and 4, the position of the antennas shift 90° in the elevation plane, as shown in the right figure.

Fig. 13 shows the directional beam pattern of the sparse cylindrical array under the condition of $M = 4$, $N = 5$ and $a = \lambda$ for the LARGE phantom, and Fig. 13 also shows the directional beam patterns of two uniform cylindrical arrays with the conditions of $M = 4$, $N = 5$ and $M = 8$, $N = 5$, for comparison. In the elevation plane, both the number of lobes and the half-power beam width are almost the same among these conditions, while the maximum magnitude of the beam patterns in the case of the sparse cylindrical array and in the case of $M = 4$, $N = 5$ are almost the same ($M = 8$: maximum value 14.7 dBi, $\varphi = 90°$; $M = 4$: maximum value 13.7 dBi, $\varphi = 45°$; Sparse array: maximum value 13.6 dBi, $\varphi = 45°$). In the $\theta = 90°$ direction the maximum magnitude is 2 dB larger than that in the case of $M = 4$ ($M = 4$: maximum value 10.7 dBi, $\theta = 90°$; Sparse array: maximum value 12.9 dBi, $\theta = 90°$). In the azimuth plane, an especially good performance of beam pattern is observed, in the case of a sparse cylindrical array. In the $\theta = 90°$ direction, the maximum magnitude is 2 dB larger than that in the case of $M = 4$ (Sparse array: maximum value 12.9 dBi, $\theta = 90°$), while two large side lobes are obtained in the $\theta = 60°$ and $\theta = 120°$ directions (Sparse array: maximum value 8.3 dBi, $\theta = 60°$ and 120°).

V. CONCLUSION

In this study, a wearable antenna array consisting of simple z-polarized dipole antennas is studied for intelligent health monitoring and prognosis. A simple cylinder is used as a human torso phantom. Two phantoms are considered to obtain a general conclusion. The antenna arrangement is considered from a one-dimensional antenna to a three-dimensional cylindrical antenna array. The results are obtained by using the electromagnetic simulation software SEMCAD.

The results show that for one circular array ($N = 1$), with an increase in the number of elements in each circular array M, the number of lobes in the elevation plane does not change when the magnitude is enhanced; in the azimuth plane, with the increase of M, the magnitude of the major lobe is enhanced and that of the side lobes is weakened. For an increase in the number of circular arrays N, the magnitude of the lobes in the elevation plane is enlarged; in the azimuth plane, with increasing N, the magnitude of the major lobe is enhanced while the half-power beam width is narrowed. In other words, the magnitude of the beam pattern increases with increasing antenna number; however, there is no linear relationship between them. In the azimuth plane, it is preferred to add elements to each circular array. In the elevation plane increasing the number of circular arrays can improve the maximum magnitude of the major lobe, but at the expense of the half-power beam bandwidth. A large magnitude of the directional beam pattern can improve the received power; however, when the human body moves or turns around, a narrow half-power beam bandwidth will reduce the quality of communication. Therefore, the number of circular arrays needs to be determined according to practical applications. The distance between circular arrays of $a = 1\lambda$ is preferred at approximately 5 GHz.

In the practical use of these guidelines for the application of intelligent wearable sensor arrays, the results in this study

are considered applicable even when the arrangement of antennas becomes complex. In this study, only the z-polarized dipole antenna is considered. The magnitude of the directional beam pattern will be enhanced under the condition that the x-, y- and z-polarized dipole antennas are used at the same time, which will be studied in the future. In this study, a simple sparse nested array is proposed and good directional beam pattern performance is obtained. A specialized study on sparse nested arrays applied in intelligent health monitoring and prognosis will also be studied in the future.

ACKNOWLEDGMENTS

The authors would like to thank Professor Qiang Chen at Tohoku University for allowing us to use the computer with the electromagnetic software SEMCAD installed in his lab.

REFERENCES

[1] P. S. Hall, and Y. Hao, *Antennas and Propagation for Body-Centric Wireless Communications*, 2nd ed., London, U.K.: Artech House, 2012, pp. 586–589.
[2] Q. Yuan and T. Ishikawa, "Effect of via-wheel power transfer system on human body," in *Proc. IEEE Wireless Power Transf. (WPT)*, Perugia, Italy, May 2013, pp. 238–241.
[3] Y. Li, H. Sato, and Q. Chen, "Capsule antenna design based on transmission factor through the human body," *IEICE Trans. Commun.*, vol. E101.B, no. 2, pp. 357–363, Feb. 2018.
[4] Y. Li, H. Sato, and Q. Chen, "FDTD analysis of capsule dipole antenna in the digestive system of a human body," *IEICE Commun. Express*, vol. 6, no. 6, pp. 276–280, Jun. 2017.
[5] Y. Li, H. Sato, and Q. Chen, "Experiment study of transmission characteristics through conducting human body equivalent liquid," *IEICE Commun. Express*, vol. 6, no. 6, pp. 286–291, Jun. 2017.
[6] Q. Liang, "Radar sensor networks for automatic target recognition with delay-Doppler uncertainty," in *Proc. IEEE Military Commun. Conf. (MILCOM)*, Tampa, FL, USA, Oct. 2006, pp. 1–7.
[7] I. Maherin and Q. Liang, "Multistep information fusion for target detection using UWB radar sensor network," *IEEE Sensors J.*, vol. 15, no. 10, pp. 5927–5937, Oct. 2015.
[8] Q. Liang, X. Cheng, S. C. Huang, and D. Chen, "Opportunistic sensing in wireless sensor networks: Theory and application," *IEEE Trans. Comput.*, vol. 63, no. 8, pp. 2002–2010, Aug. 2014.
[9] Q. Liang, "Situation understanding based on heterogeneous sensor networks and human-inspired favor weak fuzzy logic system," *IEEE Syst. J.*, vol. 5, no. 2, pp. 156–163, Jun. 2011.
[10] Q. Liang, X. Cheng, and S. W. Samn, "NEW: Network-enabled electronic warfare for target recognition," *IEEE Trans. Aerosp. Electron. Syst.*, vol. 46, no. 2, pp. 558–568, Apr. 2010.
[11] Q. Liang and X. Cheng, "KUPS: Knowledge-based ubiquitous and persistent sensor networks for threat assessment," *IEEE Trans. Aerosp. Electron. Syst.*, vol. 44, no. 3, pp. 1060–1069, Jul. 2008.
[12] D. A. Linebarger, I. H. Sudborough, and I. G. Tollis, "Design and analysis of distributed radar sensor networks," *IEEE Trans. Parallel Distrib. Syst.*, vol. 22, no. 11, pp. 1926–1933, Nov. 2011.
[13] Q. Liang, S. W. Samn, and X. Cheng, "UWB radar sensor networks for sense-through-foliage target detection," in *Proc. IEEE Int. Conf. Commun.*, San Francisco, CA, USA, May 2008, pp. 2228–2232.
[14] L. Zhao and Q. Liang, "Hop-distance estimation in wireless sensor networks with applications to resources allocation," *EURASIP J. Wireless Commun. Netw.*, vol. 2007, p. 084256, Dec. 2007.
[15] P. Pal and P. P. Vaidyanathan, "Nested arrays in two dimensions, Part II: Application in two dimensional array processing," *IEEE Trans. Signal Process.*, vol. 60, no. 9, pp. 4706–4718, Sep. 2012.
[16] P. P. Vaidyanathan and P. Pal, "Theory of sparse coprime sensing in multiple dimensions," *IEEE Trans. Signal Process.*, vol. 59, no. 8, pp. 3592–3608, Aug. 2011.
[17] Q. Liang, B. Zhang, C. Zhao, and Y. Pi, "TDoA for passive localization: Underwater versus terrestrial environment," *IEEE Trans. Parallel Distrib. Syst.*, vol. 24, no. 10, pp. 2100–2108, Oct. 2013.
[18] N. Wu and Q. Liang, "Underwater DoA estimation based on nested array," in *Proc. IEEE Military Commun. Conf. (MILCOM)*, Tampa, FL, USA, Oct. 2015, pp. 216–221.
[19] N. Wu and Q. Liang, "Underwater mobile co-prime sensor array for angle of arrival estimation based on space-domain sensor synthesis," in *Proc. IEEE Conf. Comput. Commun. Workshops*, San Francisco, CA, USA, Apr. 2016, pp. 630–635.
[20] N. Wu and Q. Liang, "Sparse nested cylindrical sensor networks for Internet of mission critical things," *IEEE Internet Things J.*, to be published.
[21] S. Gabriely, R. Lau, and C. Gabriel, "The dielectric properties of biological tissues: II. Measurements in the frequency range 10 Hz to 20 GHz," *Phys. Med. Biol.*, vol. 41, no. 11, pp. 2251–2269, 1996.
[22] S. Gabriel, R. W. Lau, and C. Gabriel, "The dielectric properties of biological tissues: III. Parametric models for the dielectric spectrum of tissues," *Phys. Med. Biol.*, vol. 41, no. 11, pp. 2271–2293, 1996.

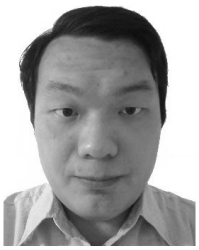

YANG LI received the B.E. and M.E. degrees from the College of Information Technology and Science, Nankai University, Tianjin, in 2008 and 2012, respectively, and the Ph.D. degree from the Department of Engineering, Tohoku University, Sendai, in 2017. He is currently with the College of Electronic and Communication Engineering, Tianjin Normal University. His research interests include antenna design, EM-wave propagation, and sensor network.

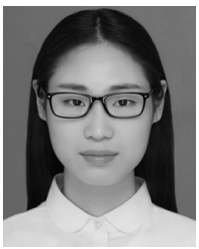

MIN ZHANG is currently pursuing the Graduation degree with the College of Electronic and Communication Engineering, Tianjin Normal University, Tianjin, China.

Her current research interests include EM-wave propagation, sensor network, heterogeneous data fusion and processing, deep learning, tensor space, and big data mining.